ORIGINAL ARTICLE

AASLD
AMERICAN ASSOCIATION FOR
THE STUDY OF LIVER DISEASES

OPEN

The S100 calcium-binding protein A6 plays a crucial role in hepatic steatosis by mediating lipophagy

Qian Du[1,2] | Tingting Zhu[3] | Guorong Wen[2] | Hai Jin[2] | Jiaxing An[2] | Jingyu Xu[2] | Rui Xie[2] | Jiaxing Zhu[2] | Xiaoxu Yang[2] | Ting Zhang[2] | Qi Liu[2] | Shun Yao[2] | Xingyue Yang[2] | Biguang Tuo[2,4] | Xiong Ma[1]

[1]Division of Gastroenterology and Hepatology, Key Laboratory of Gastroenterology and Hepatology, Ministry of Health, State Key Laboratory for Oncogenes and Related Genes, Renji Hospital, School of Medicine, Shanghai Jiao Tong University; Shanghai Institute of Digestive Disease, Shanghai, China

[2]Department of Gastroenterology, Digestive Disease Hospital, Affiliated Hospital of Zunyi Medical University, Zunyi, Guizhou, P.R. China

[3]School of Medicine, Guizhou University, Guiyang, Guizhou, China

[4]The Collaborative Innovation Center of Tissue Damage Repair and Regeneration Medicine of Zunyi Medical University, Zunyi, China

Correspondence
Biguang Tuo, Department of Gastroenterology, Affiliated Hospital of Zunyi Medical University, 149 Dalian Road, Huichuan, Zunyi, Guizhou 563003, P.R. China.
Email: tuobiguang@aliyun.com

Xiong Ma, Renji Hospital, School of Medicine, Shanghai Jiao Tong University; Shanghai Institute of Digestive Disease, 145 Middle Shandong Road, Shanghai 200001, China.
Email: maxiongmd@ hotmail.com

Abstract

Background: S100 calcium-binding protein A6 (S100A6) is a calcium-binding protein that is involved in a variety of cellular processes, such as proliferation, apoptosis, and the cellular response to various stress stimuli. However, its role in NAFLD and associated metabolic diseases remains uncertain.

Methods and Results: In this study, we revealed a new function and mechanism of S100A6 in NAFLD. S100A6 expression was upregulated in human and mouse livers with hepatic steatosis, and the depletion of hepatic S100A6 remarkably inhibited lipid accumulation, insulin resistance, inflammation, and obesity in a high-fat, high-cholesterol (HFHC) diet-induced murine hepatic steatosis model. In vitro mechanistic investigations showed that the depletion of S100A6 in hepatocytes restored lipophagy, suggesting S100A6 inhibition could alleviate HFHC-induced NAFLD. Moreover, S100A6 liver-specific ablation mediated by AAV9 alleviated NAFLD in obese mice.

Conclusions: Our study demonstrates that S100A6 functions as a positive regulator of NAFLD, targeting the S100A6-lipophagy axis may be a promising treatment option for NAFLD and associated metabolic diseases.

INTRODUCTION

NAFLD is one of the major chronic liver diseases worldwide, which encompasses a broad spectrum of conditions from simple hepatic steatosis to fibrosis, cirrhosis and HCC. NAFLD significantly increases the risk of cardiovascular diseases and type 2 diabetes mellitus.[1,2] Accumulating studies demonstrate that hepatic steatosis is not only linked to inflammation, insulin resistance, and obesity but also affects liver-related mortality or morbidity.[3,4] Unfortunately, the progression of hepatic steatosis is not fully understood, and there are still no effective pharmacological therapies for NAFLD. The tasks of developing novel therapeutics are urgently needed to further reduce the burden of NAFLD.

The abnormal lipid accumulation in hepatocytes is believed to be the beginning of hepatic steatosis. Free fatty acids are taken up by hepatocytes and converted into triglycerides (TG) for storage as lipid droplets (LDs). Normally, LDs are degraded through hydrolysis, which is catalyzed by the PLIN1-hormone-sensitive lipase–monoglyceride lipase axis,[5–7] and lipophagy.[8] However, excessive intake of free fatty acids results in the abundance of intracellular LDs, which causes lipotoxicity and further promotes ER stress, apoptosis, and inflammation.[9] As the major perpetrators of lipotoxic injuries to hepatocytes, LD clearance is important for the maintenance of liver function. Autophagy, as an important part of cell metabolism, is the "recycling station" in cells that contributes to maintaining cellular homeostasis by breaking down abnormal and redundant substances and providing materials for the reconstruction of new molecules. In the past decade, accumulating evidence has shown that lipophagy, which is the process of selective degradation of LDs through autophagy, is impaired in the livers of NAFLD patients.[10,11] Previous studies have suggested that exercise and dietary intervention could alleviate NAFLD by promoting lipophagy.[12] Pharmacological inhibition of lipophagy significantly decreased the lipolytic breakdown of TG and cholesterol from LDs, leading to increased liver steatosis after a lipid challenge.[13] However, the role of lipophagy in the pathogenesis of NAFLD remains controversial.

S100 calcium-binding protein A6 (S100A6) is a member of the S100 protein family of calcium-binding proteins, which is mainly involved in the regulation of proliferation, apoptosis, cytoskeleton dynamics, and cellular responses to different stressors.[14–16] S100A6 can also be secreted or released by various cell types, indicating that the protein has extracellular effects.[16] In previous studies, S100A6 expression was elevated in hepatocytes, gastric and pancreatic malignant tissues and was regarded as a diagnostic marker or prognostic factor for pancreatic cancer, gastric cancer, and HCC.[17–19] Researchers discovered that palmitic acid and oleic acid (OA) upregulated the expression of S100A6 in their examination of the effects of chronic lipid exposure on pancreatic beta-cell function.[20] Based on this observation, we wonder whether S100A6 can regulate fat metabolism in addition to its role in cancers.

The present study sought to provide new evidence that S100A6 is involved in NAFLD and related metabolic disorder regulation. S100A6 expression was remarkably increased in the livers of mice with steatosis and related hepatic diseases. Hepatocyte S100A6-deficient mice were protected against high-fat high-cholesterol (HFHC)-induced steatosis and showed improved insulin sensitivity. Mechanistically, S100A6 served as an essential regulator of NAFLD by modulating lipophagy. These data provide evidence for the major role of hepatic S100A6 and its related functional pathway in HFHC-induced liver steatosis.

METHODS

Animals

All experiments were approved by the Institute of Animal Care and Use Committee of the Affiliated Hospital of Zunyi Medical University. Experimental animals (C57BL/6, 6–8 wk, male) were purchased (from the Beijing HFK, China) and housed in the Laboratory Animal Center, Digestive Disease Institute of Guizhou Province, Affiliated Hospital of Zunyi Medical University.

Adult male mice (C57BL/6) of 8–10 weeks of age were housed at 25°C $\pm$ 5°C under a 12 h light/dark cycle with free access to water and food. The mice were fed a high-fat diet (60% fat, 20% carbohydrate, and 20% protein, trophic diets) for 22 weeks, a HFHC (42% fat and 0.2% cholesterol; trophic diets) diet for 24 weeks, and methionine-choline deficient diet (22% fat, 63% carbohydrate, and 14.6% protein) for 8 weeks. A normal chow diet (CD) (4% fat, 78% carbohydrate, and 18% protein) was used as a control. Before the formal experiment, the mice were adaptively fed the control diet for 2 weeks. We killed the mice at the 22nd and 24th weeks of food induction, respectively, and collected liver tissues for follow-up studies. The *ob/ob* and *db/db* mice were fed a CD diet for 8 weeks, and more detailed information on *ob/ob* and *db/db* mice can be found in Supplemental Data Table 1, http://links.lww.com/HC9/A452.

For specific S100A6 knockdown mice, 7-week-old mice were injected with 1×10^{12} (100 μl) genome copies of adeno-associated viral serotype 9 (AAV9) encoding a control shRNA or S100A6 shRNA (Hanbio Biotechnology, Shanghai, China). More detailed information can be found in Supplemental Data Table 2, http://links.lww.com/HC9/A452. The sequence of shRNA targeting S100A6 was 5-GCTTTGATCTACAATGAAGCT-3. All

mice were fed an HFHC diet after tail vein injection. Body weight and blood glucose concentrations were monitored weekly in all mice. After 15 weeks of feeding, the mice were killed, and serum and liver tissues were collected and stored at −80°C for further experiments.

Cell culture and treatment

Normal human hepatocyte LO2 cells were purchased from the Center for Type Culture Collection, China, and HepLi5 cells were from the State Key Laboratory for Diagnosis and Treatment of Infectious Diseases, First Affiliated Hospital, School of Medicine, Zhejiang University, Hangzhou China.[21] The cells were cultured in a standard medium comprising DMEM (XP BioMed., C3113-0500), 10% FBS (XP BioMed, C04001-500), and 1% penicillin-streptomycin and were maintained in a humidified 5% CO_2 atmosphere in a cell incubator at 37°C. When the cell density reached 70%–80%, the cells were used for experiments.

Palmitic acid (PA) (Sigma, P0500) was dissolved in a mixture of 0.1 mol/L NaOH and 20% BSA at a stock concentration of 20 mM and added to DMEM containing 1% BSA to ensure a physiological ratio between bound and unbound PA in the medium. OA (Aladdin, O108485) was dissolved in a mixture of 0.1 mol/L NaOH and 10% BSA at a stock concentration of 50 mM. To establish a model of lipid accumulation in vitro in HepLi5 and LO2 cells, a mixture of PA (0.5 mM) and OA(0.1 mM, 0.2 mM, 0.3 mM) was added for 24 h. Chloroquine (CQ) (MCE, HY-17589A) was administered for 6 h at a concentration of 20 μM, which was used as a positive control for autophagosome accumulation.

Lentivirus infection

Hanheng Biotechnology was commissioned to construct and package the S100A6 knockdown lentivirus vector (pHBLV-U6-MCS-CMV-ZsGreen-PGK-PURO, HH20210 923ZJ). The shS100A6 target sequences were as follows 5′-GTGCAAGGCTGATGGAAGACTT-3′ and 5′-AAGTC TTCCATCAGCCTTGCAC-3′. LO2 or HepLi5 cells were infected at a multiplicity of infection of 50 with lentivirus knockdown of S100A6 according to the manufacturer's protocol. The HBLV-PURO vector was used as a negative control, and more detailed information can be found in Supplemental Data Table 7, http://links.lww.com/HC9/A452. The protein levels of S100A6 were examined by Western blotting and real-time quantitative PCR (qPCR).

Biochemistry assay

For animals, the serum levels of TG (Nanjing Jiancheng, A110-1-1), total cholesterol (TC) (Nanjing Jiancheng, A111-1-1), alanine aminotransferase (Nanjing Jiancheng, A059-2-2), and aspartate aminotransferase (Nanjing Jiancheng, C010-2-1) were measured using colorimetric diagnostic kits according to the manufacturer's instructions. The intrahepatic TG and TC levels were measured according to the methods of commercial kits. The level of liver lipids was normalized to the protein concentrations. For LO2 and HepLi5 cells, cultured LO2 and HepLi5 cells were collected by centrifugation at 12000 rpm for 30 min at 4°C after treatment with PA/OA (0.5/0.2 mM) for 24 h and/ or CQ (chloroquine) (25 μM) for 6 h. The intrahepatic TG, and TC levels were measured according to the methods of commercial kits.

Metabolic assays

Glucose tolerance tests and insulin tolerance tests were performed by i.p. injection of 1 g/kg glucose and 0.75 U/ kg insulin into the mice after 6 hours of fasting. Blood glucose levels were detected at 0, 30, 60, 90, and 120 min after injection. The AUC was calculated to reflect glucose and insulin tolerance levels.

Autophagic flux quantification

mCherry-LC3 stable HepLi5 and LO2 cells were seeded in 96-well plates, and then treated with PA/OA (0.25 mM/ 0.1 mM) for 16 h and/or CQ (25 μM) for 6 h. The cells were fixed with 4% paraformaldehyde before they were washed with PBS and embedded using DAPI. Images were acquired using a high-connotation imaging analysis system.

Real-time quantitative PCR

Total RNA was extracted from liver tissue or cultured cells using TransZol Up Reagent (TransGen Biotech, ET111-01) and then reverse transcribed to cDNA using the EasyScript One-step gDNA Removal Kit (TransGen Biotech, AE311-04) for qPCR. TransStart Top Green qPCR Super Mix (TransGen Biotech, AQ131-04) was used to quantify PCR amplification. Relative gene expression was calculated with the $2^{-\Delta\Delta C}$ method and normalized to β-actin expression. The primers used in this study are listed in Supplemental Data Table 3, http://links.lww.com/HC9/A452 and Table 4, http://links.lww.com/HC9/A452.

Western blot analysis

Total protein was isolated from tissues or cells in ice-cold Plus RIPA Lysis Buffer (Boster, AR0102), and protein concentrations were determined using an *Easy* II Protein Quantitative Kit (BCA) (TransGen Biotech, DQ111-01). A total of 40–60 μg of protein was loaded into 10% SDS–

PAGE gels, transferred to a polyvinylidene difluoride membrane and incubated with corresponding primary antibodies overnight at 4°C. After incubation with peroxidase-conjugated secondary antibodies, a chemiluminescence system was used for signal detection. Protein expression levels were normalized to the housekeeping gene GAPDH (Abcam, ab8245). The indicated antibodies are listed in Supplemental Data Table 5, http://links.lww.com/HC9/A452 and Table 6, http://links.lww.com/HC9/A452.

Histological analysis

Tissue fixed in 4% paraformaldehyde was embedded in paraffin by using standard procedures. Paraffin-embedded liver sections were stained with H&E after deparaffinization and rehydration to assess the distribution of lipid accumulation. Images were acquired with a light microscope. For periodic acid-Schiff staining (Solarbio, G1281), paraffin-prepared liver sections were dewaxed using conventional methods and hydrated in distilled water and then incubated in oxidant for 8 min at room temperature, followed by washing and incubating the sections in Schiff reagent in the dark place for 18 min. Thereafter, Mayer hematoxylin solution was used to stain the nuclei, and the sections were differentiated using an acidic differentiation solution and dehydrated using a series of ethanol gradients. Finally, the sections were cleared with xylene and sealed with resin.

Oil Red O staining

For the staining of LDs, LO2 or HepLi5 cells were cultured in media containing PA/OA (0.25 mM/0.1 mM) or PA/OA (0.25 mM/0.1 mM) and CQ (25 μM). The cells were incubated with PA/OA for 16 h and CQ for 6 h. Then, the cells were washed twice with PBS, fixed with 4% formaldehyde in distilled water, and incubated overnight at 4°C. Afterward, the formaldehyde solution was removed. Then, the cells were washed 3 times with PBS, and washed once with 60% isopropanol for 2 min. Cells were incubated with a 0.3% Oil Red O solution (Sigma, 1320-06-5) in 60% isopropanol for 10 min at 37°C. The Oil Red O solution was discarded. Counterstaining of cell nuclei was performed using hematoxylin incubation. Stained cells were washed twice with PBS and covered with glycerol. Analysis was carried out using a microscope. For unfixed cryosections, unfixed frozen sections were washed once with distilled water, treated with 60% isopropanol for 1 minute, and stained with 0.3% Oil Red O solution in 60% isopropanol for 10 min at 37°C. Stained unfixed frozen sections were washed 3 times with 60% isopropanol and 3 times with distilled water. Counterstaining of cell nuclei was performed with hematoxylin culture. Stained sections were covered with glycerol and observed by microscope.

BODIPY 493/503 staining of LDs

The cells were treated as described above. The cells were fixed with 4% paraformaldehyde overnight at 4°C. and subsequently stained with 2 μM BODIPY 493/503 (Invitrogen, D3922) at room temperature in the dark 10 min. Then the cells were sealed with a fluorescent mounting medium containing DAPI (Boster, AR1176). Images were observed using a high-connotation imaging analysis system (PerkinElmer, USA).

Statistical analyses

The experimental data were statistically analyzed by SPSS 17.0 software, and the data are expressed as the mean $\pm$ SEM. The paired samples were tested by paired Student t test, and the data were compared by single factor ANOVA. The data were plotted by GraphPad Prism 7 software, and the significance levels were *$p < 0.05$, **$p < 0.01$ and ***$p < 0.001$.

RESULTS

S100A6 expression was upregulated in hepatic steatosis

To investigate the involvement of S100A6 in hepatic steatosis, both the mRNA and protein expression levels of S100A6 in the liver tissues of mice with NAFLD were analyzed. As shown in Figure 1A and B, significantly higher S100A6 protein levels were observed in the livers of wild-type mice with HFHC-induced hepatic steatosis. In addition, the same expression pattern of S100A6 was found in the livers of high-fat diet and methionine-choline deficient-induced NAFLD model mice as in HFHC treatment (Figure 1C–F). Furthermore, obviously higher S100A6 expression levels were observed in the livers of NAFLD patients than in healthy controls (Figure 1G). The experimental results from the cultured human hepatocyte cell lines also showed that PA/OA concentration dependently stimulated the increase of S100A6 expression in both LO2 and HepLi5 cells (Figure 1H–J, Supplemental Figures 1A-1B, http://links.lww.com/HC9/A453).

A comprehensive analysis of data from other liver injury models in the GEO database was performed to further evaluate the S100A6 expression in liver disease model animals. Consistent with our findings, the levels of S100A6 were significantly increased in the mice treated with the Western diet, CCl$_4$/ethyl alcohol, or a 3,5-diethoxycarbonyl-1,4-dihydrocrolidine diet (Supplemental Figure 1C, http://links.lww.com/HC9/A453). Interestingly, high levels of S100A6 were also seen in HCC and cholangiocarcinoma (Supplemental Figure 1D, http://links.lww.com/HC9/A453). Overall, the above evidence showed a significant increase of S100A6 in the context
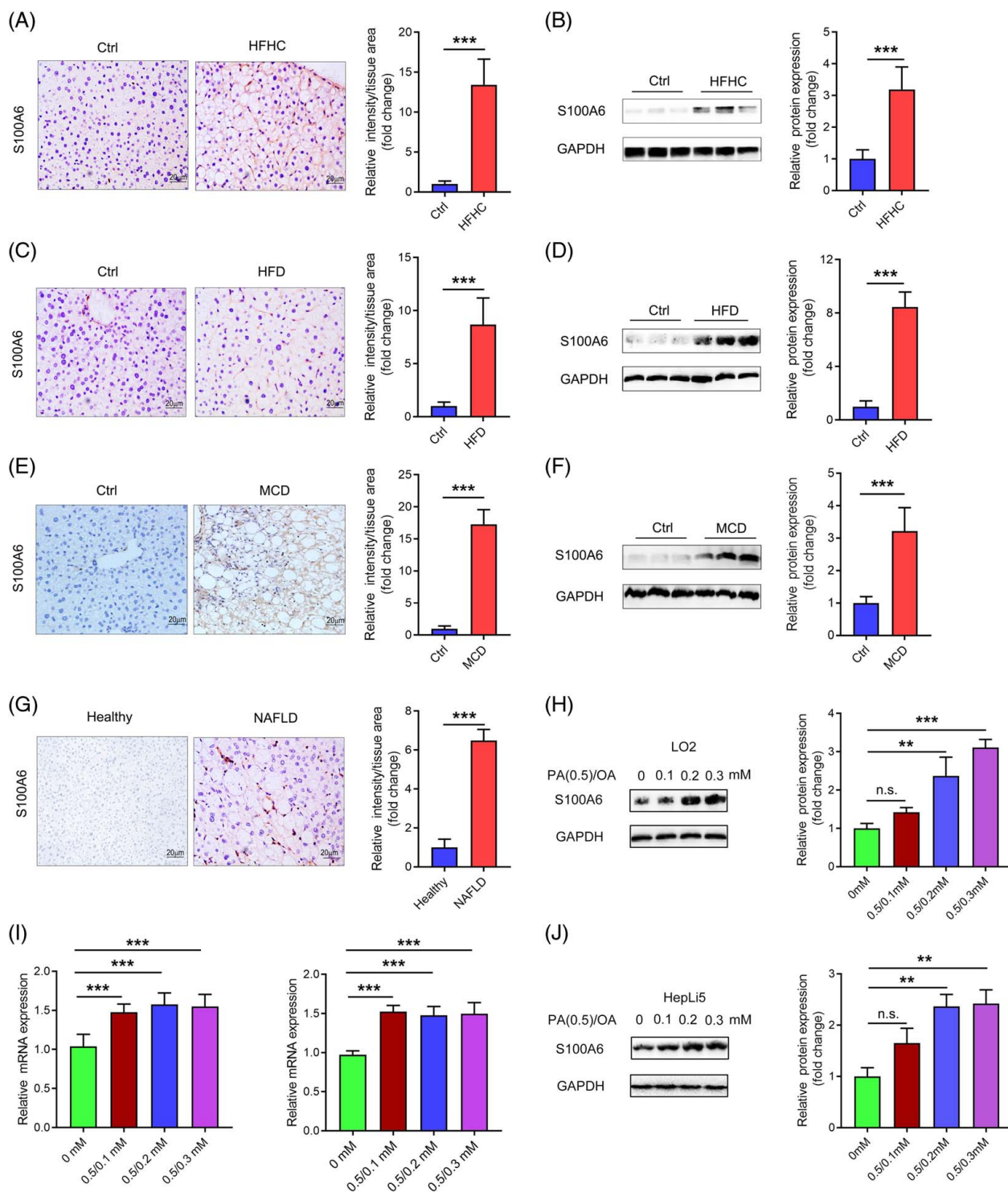
FIGURE 1 S100A6 expression was upregulated in the fatty liver. (A) Images of immunohistochemical staining for S100A6 in the liver sections of C57BL/6J mice fed an HFHC diet or CD for 24 weeks (n = 8 per group). Scale bar, 20 μm. (B) S100A6 protein expression in the liver samples of mice that were fed an HFHC diet or CD by Western blotting analysis. (C) Immunohistochemical staining of S100A6 in C57BL/6J mice fed an HFD or CD for 22 weeks (n = 8 per group). Scale bar, 20 μm. (D) S100A6 protein expression in HFD-treated mice by Western blotting analysis. (E) Immunohistochemical staining of S100A6 in C57BL/6J mice fed an MCD or CD for 8 weeks (n = 8 per group). Scale bar, 20 μm. (F) S100A6 protein expression in MCD-treated mice by Western blotting analysis. (G) Immunohistochemical staining of S100A6 in the liver tissues of healthy individuals and individuals with hepatic steatosis. Scale bar, 20 μm. (H) S100A6 protein levels in LO2 cells treated with PA/OA (0.5/0.1, 0.5/0.2, 0.5/0.3 mM) or BSA for 24 h by Western blotting analysis.(I) mRNA levels of S100A6 in the human hepatocyte cell line LO2 (left) and HepLi5 cells (right) treated with PA/OA (0.5/0.1 mM, 0.5/0.2 mM, 0.5/0.3 mM) or BSA for 24 h. (J) S100A6 protein levels in HepLi5 cells treated with PA/OA (0.5/0.1, 0.5/0.2, 0.5/0.3 mM) or BSA for 24 h by Western blotting analysis. Data are expressed as the mean ± SEM. $^{**}p < 0.01$, $^{***}p < 0.001$ and n.s. indicates no significance. Abbreviations: CD, chow diet; HFD, high-fat diet; HFHC, high-fat high-cholesterol; MCD, methionine-choline deficient; OA, oleic acid.

of NAFLD and related liver diseases, suggesting that S100A6 might play a role in the development of NAFLD.

S100A6 deficiency reduced PA/OA-induced lipid accumulation in LO2 and HepLi5 cells

The upregulation of S100A6 expression in hepatic steatosis prompted us to explore the functional role of S100A6 in lipid metabolism. S100A6 was knocked down in both LO2 and HepLi5 cells using lentivirus, and the infection efficiency was tested using mRNA and protein analyses (Figure 2A and F and Supplemental Figure 2A and 2B, http://links.lww.com/HC9/A453). The 2 cell lines were treated with PA/OA before harvesting. As shown in Figure 2B and G, treatment with PA/OA significantly decreased the TG levels in S100A6 knockdown cells compared with cells expressing the vector alone. Both BODIPY 493/503 and Oil Red O staining consistently confirmed that the number of LDs was also less in the shS100A6 groups than in controls (Figure 2C, D, H, and I). The imbalance of lipid biosynthesis, lipolysis, uptake, and efflux is the primary cause of abnormal lipid accumulation. We further examined the protein and mRNA levels of well-known genes involved in the biosynthesis of TG and CE (cholesterol esters), such as acetyl-CoA carboxylase 1, fatty acid synthase, stearoyl-CoA desaturase 1, acyl-CoA oxidase 1, carnitine palmitoyl transferase 1 alpha, and 3-hydroxy-3-methylglutaryl-CoA reductase. The results showed that the protein and mRNA levels of acetyl-CoA carboxylase 1, fatty acid synthase, stearoyl-CoA desaturase 1, acyl-CoA oxidase 1, carnitine palmitoyl transferase 1 alpha, and 3-hydroxy-3-methylglutaryl-CoA reductase were significantly decreased in the PA/OA-treated S100A6 knockdown groups compared with the control (shCtrl) group (Figure 2E and J). Take together, these results convincingly support that S100A6 was critical for PA/OA-induced lipid accumulation in LO2 and HepLi5 cells.

Hepatocyte S100A6 deficiency ameliorated HFHC-induced hepatic steatosis

To further determine whether S100A6 in hepatocytes is critical for liver steatosis in vivo, AAV9 vectors were generated to deplete the S100A6 gene from the hepatocytes in mice. The mice were then subjected to HFHC treatment for 14 weeks (Figure 3A). The representative Western blots showed that S100A6 expression was sufficiently blocked in the liver tissues subjected to AAV9-shS100A6 injection compared with that in the liver tissues of AAV9-Ctrl mice (Figure 3B). Compared with AAV9-Ctrl mice, AAV9-shS100A6 mice exhibited a significant amelioration of HFHC-induced

hepatic steatosis (Figure 3C). Oil Red O staining showed that hepatic lipid accumulation was sharply decreased in the AAV9-shS100A6 group compared with the AAV9-Ctrl group after HFHC diet administration (Figure 3D).

The examination of lipid content (TG; TC; and HDL-c and LDL-c) in the serum of HFHC-induced AAV9-Ctrl or AAV9-shS100A6 mice further confirmed the amelioration effect of hepatocyte S100A6 deficiency on hepatic function (Figure 3E–H). Consistent with these findings, the intracellular TG and TC levels in murine livers were also significantly reduced by hepatic S100A6 deficiency (Figure 3I and J). Moreover, treatment of mice with AAV9-shS100A6 markedly downregulated the expression of lipid metabolic genes in the liver, including fatty acid synthase, peroxisome proliferator-activated receptor gamma, stearoyl-CoA desaturase 1, and sterol regulatory element-binding transcription factor 1. (Figure 3K). However, the expression of these lipid metabolic genes in the liver was not significantly altered in the CD-treated AAV9-shS100A6 mice in comparison with the CD-treated AAV9-Ctrl mice (Supplemental Figures 3, http://links.lww.com/HC9/A453). These data suggest that hepatocyte S100A6 deficiency ameliorated HFHC-induced hepatic steatosis, indicating that S100A6 contributes to the pathogenesis of hepatic steatosis.

S100A6 deficiency inhibited obesity and insulin resistance induced by the HFHC diet

Given that S100A6 deficiency ameliorated HFHC-induced hepatic steatosis, we further investigated whether S100A6 knockdown could decrease hepatic steatosis-related obesity and insulin resistance. In response to the HFHC treatment, the body weight of AAV9-Ctrl mice significantly increased after 14 weeks compared with that of the CD-treated group, whereas the S100A6 deficiency mice gained markedly less weight (Figure 4A).

In terms of the effect of S100A6 deficiency on insulin resistance, it was found that fasting blood glucose levels were significantly lower in AAV9-shS100A6 mice than in AAV9-Ctrl mice after HFHC diet administration (Figure 4B). In addition, the AUCs obtained from glucose tolerance tests and insulin tolerance tests assays were increased in HFHC-treated AAV9-Ctrl mice compared with the CD-treated mice, and the effects were markedly ameliorated by S100A6 deficiency (Figure 4C–F). Moreover, the level of glycogen was greatly decreased in AAV9-shS100A6 mice after HFHC diet administration (Figure 4G). Overall, the above results in the S100A6-deficient mice indicated that hepatic deficiency of S100A6 could reverse HFHC-induced obesity, insulin resistance, and glucose metabolic disturbance.
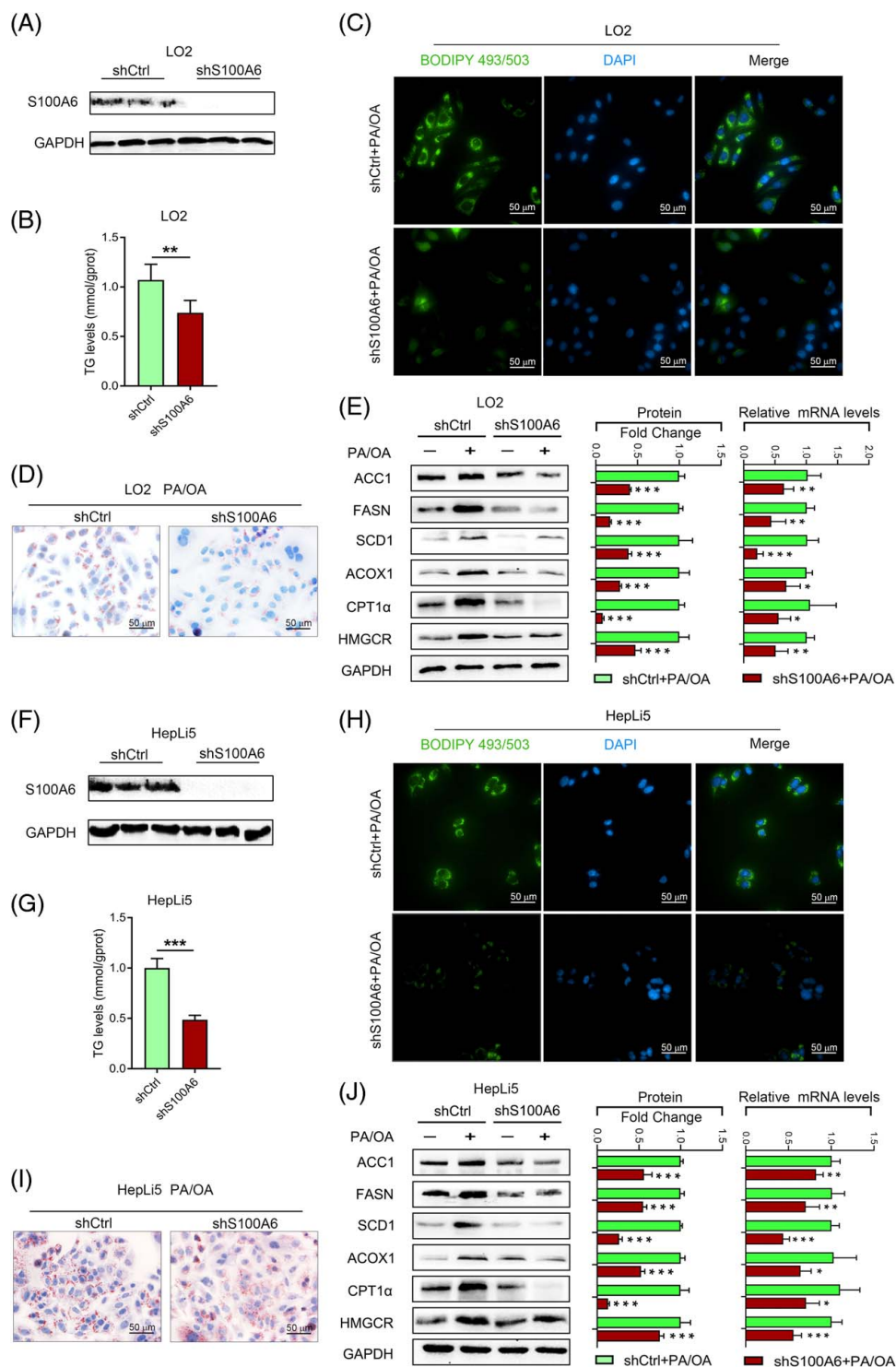
FIGURE 2 S100A6 deficiency reduced PA/OA-induced lipid accumulation in LO2 and HepLi5 cells. (A) The protein expression of S100A6 in S100A6 knockout LO2 cells by Western blotting analysis. (B) The intracellular TG levels in S100A6 knockdown or control LO2 cells after treatment with PA/OA. (C) BODIPY 493/503 and (D) Oil Red O staining of S100A6 knockdown or control LO2 cells treated with PA/OA (0.25/0.1 mM) for 24 h. Scale bar, 20 μm. (E) Relative protein and mRNA levels of lipid metabolism-related genes in S100A6 knockdown or control LO2 cells after treatment with PA/OA (protein expression: n = 3; mRNA expression: n = 6 independent experiments). (F) S100A6 protein expression in S100A6 knockout HepLi5 cells by Western blotting analysis. (G) The intracellular TG levels in S100A6 knockdown expression or control HepLi5 cells after treatment with PA/OA. (H) BODIPY 493/503 and (I) Oil Red O staining of S100A6 knockdown or control HepLi5 cells treated with PA/OA (0.25/0.1 mM) for 24 h. Scale bar, 20 μm. (J) Relative protein and mRNA levels of lipid metabolism-related genes in S100A6 knockdown or control HepLi5 cells after treatment with PA/OA (protein expression: n = 3; mRNA expression: n = 6 independent experiments). Data are expressed as the mean ± SEM. *$p < 0.05$, **$p < 0.01$, ***$p < 0.001$. Abbreviations: OA, oleic acid; PA, palmitic acid; TG, triglycerides.
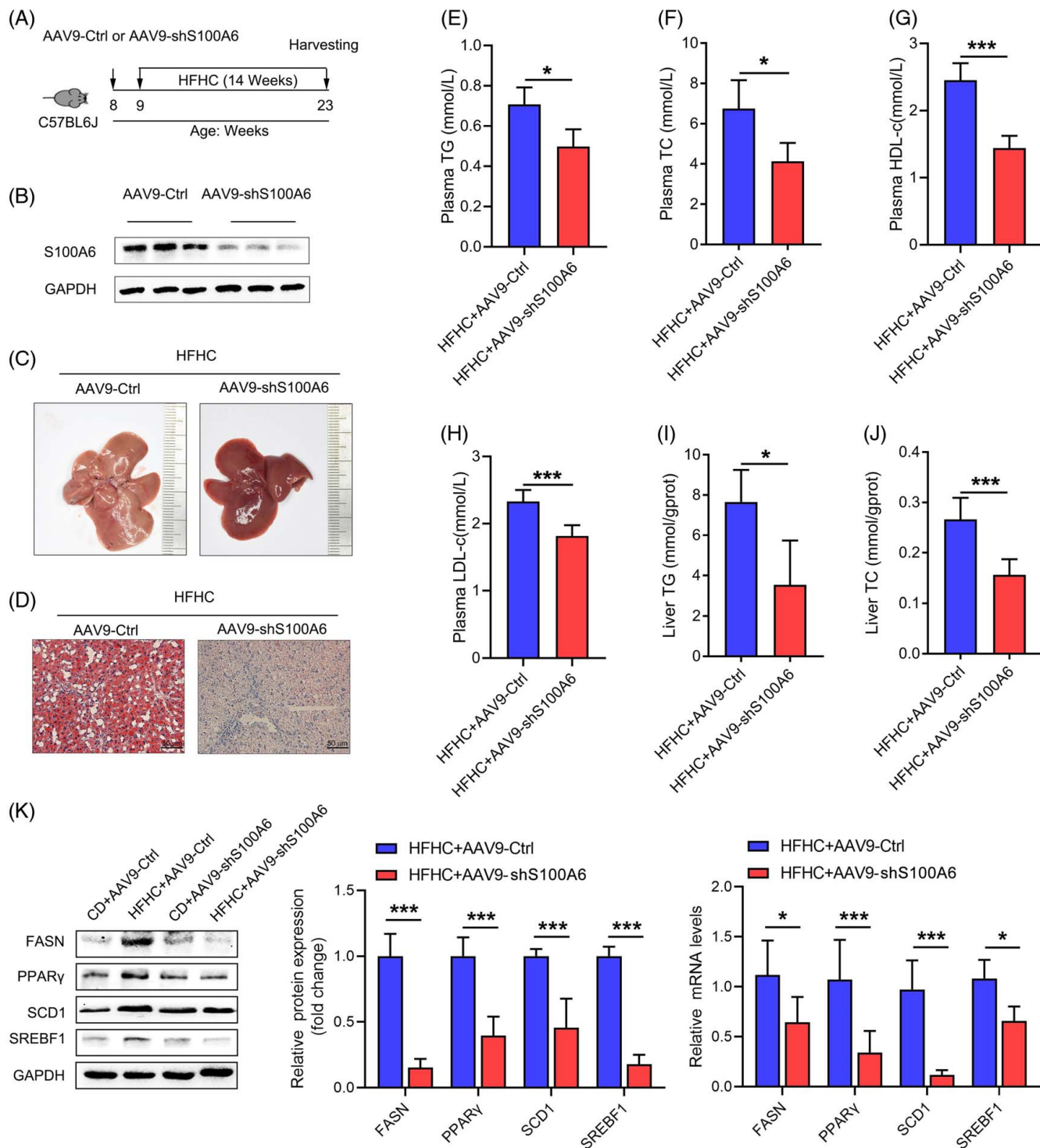
FIGURE 3 Hepatocyte S100A6 deficiency ameliorated HFHC-induced hepatic steatosis. (A) Schematic of the experimental procedure. C57BL/6J mice were injected with AAV9-Ctrl or AAV9-shS100A6 adeno-associated virus for 1 week followed by HFHC treatment for 14 weeks. (B) S100A6 expression in AAV9-Ctrl or AAV9-shS100A6 mice by Western blotting analysis. (C) Gross liver appearance. Scale bar, 1 cm. (D) Oil Red O staining in the liver sections from AAV9-Ctrl or AAV9-shS100A6 mice. Scale bar, 50 μm. (E) Serum TG, (F) TC, (G) HDL-c and (H) LDL-c levels in AAV9-Ctrl or AAV9-shS100A6 mice. (I) TG and (J) TC levels in the livers of AAV9-Ctrl or AAV9-shS100A6 mice. (K) The relative protein and mRNA levels of lipid metabolic genes in AAV9-Ctrl or AAV9-shS100A6 mice. Data are expressed as the mean ± SEM. $*p < 0.05$, $***p < 0.001$. Abbreviations: HFHC, high-fat high-cholesterol; TC, total cholesterol; TG, triglycerides.
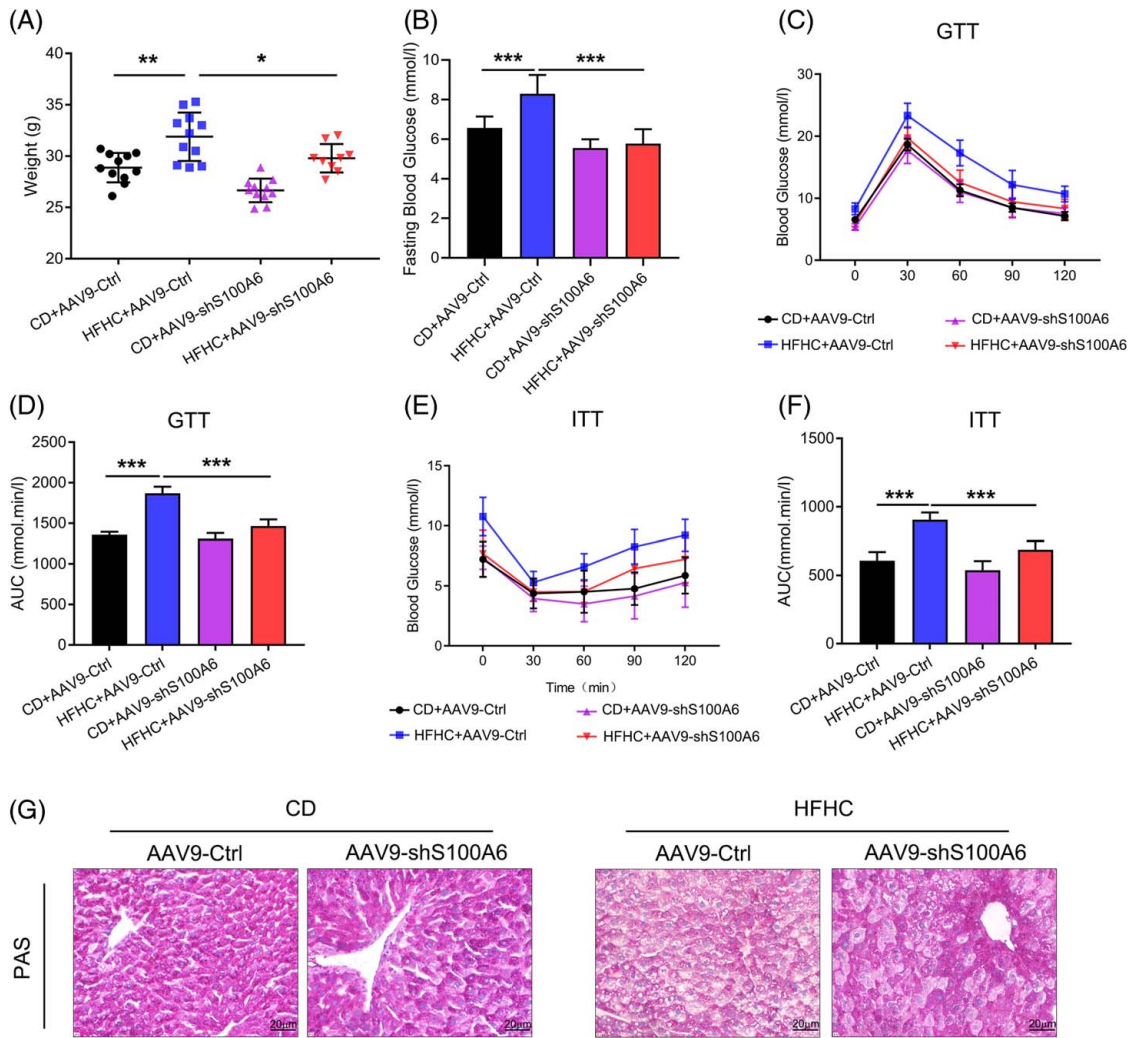
FIGURE 4 S100A6 deficiency inhibited HFHC-induced obesity and insulin resistance. (A) Body weights of S100A6 knockdown mice or their controls after 14 weeks of CD or HFHC feeding. (B) Fasting blood glucose levels in CD-fed or HFHC-fed AAV9-Ctrl or AAV9-shS100A6 mice after 14 weeks. (C) Time course of GTT, (D) AUC of GTT. (E) time course of ITT and (F) AUC of ITT. (G) The glycogen levels in the liver samples of AAV9-Ctrl or AAV9-shS100A6 mice after a 14-week HFHC treatment by PAS staining. Data are expressed as the mean $\pm$ SEM. *$p < 0.05$, **$p < 0.01$, ***$p < 0.001$. Abbreviations: HFHC, high-fat high-cholesterol; GTT, glucose tolerance tests; ITT, insulin tolerance tests.

Hepatocyte S100A6 deficiency ameliorated HFHC-induced inflammatory response

We further investigated the effect of S100A6 on HFHC-induced inflammatory response in the liver. The results showed that S100A6 deficiency by AAV9-shS100A6 significantly improved the inflammatory response induced by the HFHC diet, which was associated with increased production of anti-inflammatory mediator IL-10 (Figure 5A). In addition, the gene associated with inflammation (CCL2) was downregulated (Figure 5A). Consistent with these analyses, a positive correlation between macrophage marker CD44 and S100A6 mRNA levels was observed in HCC patients from the The Cancer Genome Atlas database (Figure 5B). In addition, a significant decrease in the serum alanine aminotransferase and

aspartate aminotransferase levels was observed in shS100A6 mice compared with Ctrl mice after the HFHC diet treatment (Figure 5C and D). However, the levels of fibrosis-related genes were not significantly affected by S100A6 levels after the short-term HFHC treatment (Figure 5E). Collectively, these findings demonstrated that hepatocyte S100A6 deficiency ameliorates HFHC-induced inflammatory responses.

S100A6 regulated hepatic steatosis through autophagy-dependent mechanism

Subsequently, to explore the mechanisms underlying the regulatory effects of S100A6 on the progression of NAFLD, RNA sequencing (RNA-Seq) analysis was performed on liver samples from AAV9-Ctrl and
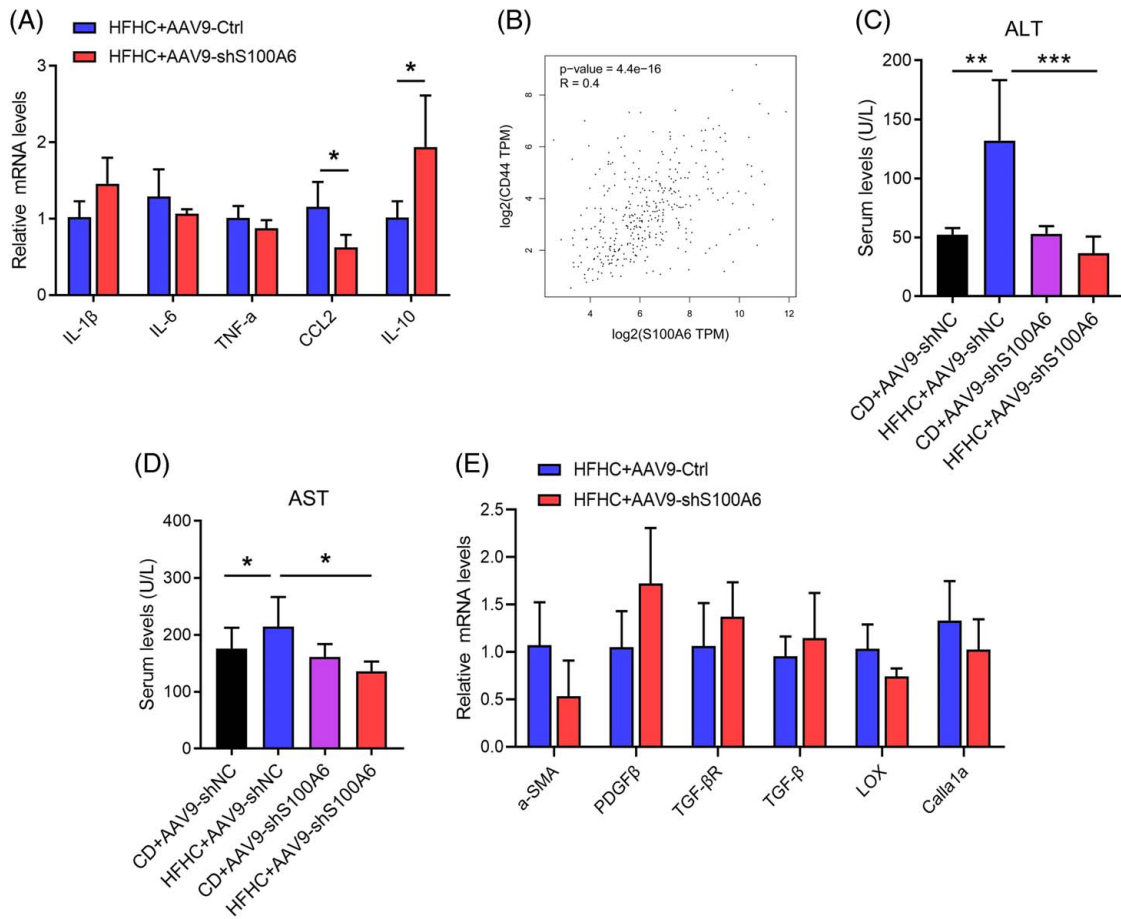
FIGURE 5 Hepatocyte S100A6 deficiency ameliorated HFHC-induced inflammatory response. (A) The relative mRNA levels of inflammation-related genes in AAV9-Ctrl or AAV9-shS100A6 mice after 14 weeks of CD or HFHC feeding. (B) A correlation between macrophage marker CD44 and S100A6 mRNA levels was observed in HCC patients from the The Cancer Genome Atlas database. Serum ALT (C) and AST (D) levels in AAV9-Ctrl or AAV9-shS100A6 mice. (E) The relative mRNA levels of fibrosis-related genes in AAV9-Ctrl or AAV9-shS100A6 mice. Data are expressed as the mean ± SEM. *$p < 0.05$, **$p < 0.01$, ***$p < 0.001$. Abbreviations: ALT, alanine aminotransferase; AST, aspartate aminotransferase; CD, chow diet; HFHC, high-fat high-cholesterol.

AAV9-shS100A6 HFHC-treated mice, and the experimental strategy is shown in Figure 6A. The criteria for the selection of genes with different expression patterns were (i) Log2 (fold change) of gene expression >1 or <−1 and (ii) adjusted p value < 0.05. As depicted in Figure 6B, 72 downregulated and 117 upregulated genes were obtained. According to the Gene Ontology analysis, 6 of the top 7 enriched biological processes related to S100A6 function were lipid metabolism-related processes (Figure 6C). Interestingly, RNA-Seq data analysis showed that the majority of genes involved in autophagy displayed a tendency of upregulation in the HFHC + shS100A6 group compared with the HFHC + Ctrl group (Figure 6D and E). Previous studies showed that the activation of autophagy could regulate the process of lipid metabolism.[22–24] Similar conclusions were obtained in our study, which showed that blocking autophagy with CQ could enhance the accumulation of LDs in both LO2 cells and HepLi5 cells, while the

use of rapamycin to activate autophagy could alleviate the accumulation of LDs in cells. Similarly, the trend in TG levels was consistent with these findings (Figures S5A-S5D, http://links.lww.com/HC9/A453). To further confirm whether S100A6 mediates the lipid accumulation through the autophagy pathway, the protein levels of autophagy markers p62 and LC3 in both PA/OA-treated or control-treated S100A6-knockdown LO2 and HepLi5 cells were evaluated. Compared with the control group, the intracellular LC3II expression was significantly upregulated after the S100A6 knockdown and the expression of p62 was also restored (Figure 6G and I, Figures S5E and S5F, http://links.lww.com/HC9/A453). In addition, increased autophagy was observed in AAV9-shS100A6 mice after HFHC treatment (Figure 6F and Figure S5G, http://links.lww.com/HC9/A453). These results suggest that S100A6 deficiency enhances autophagy under PA/OA or HFHC diet administration.
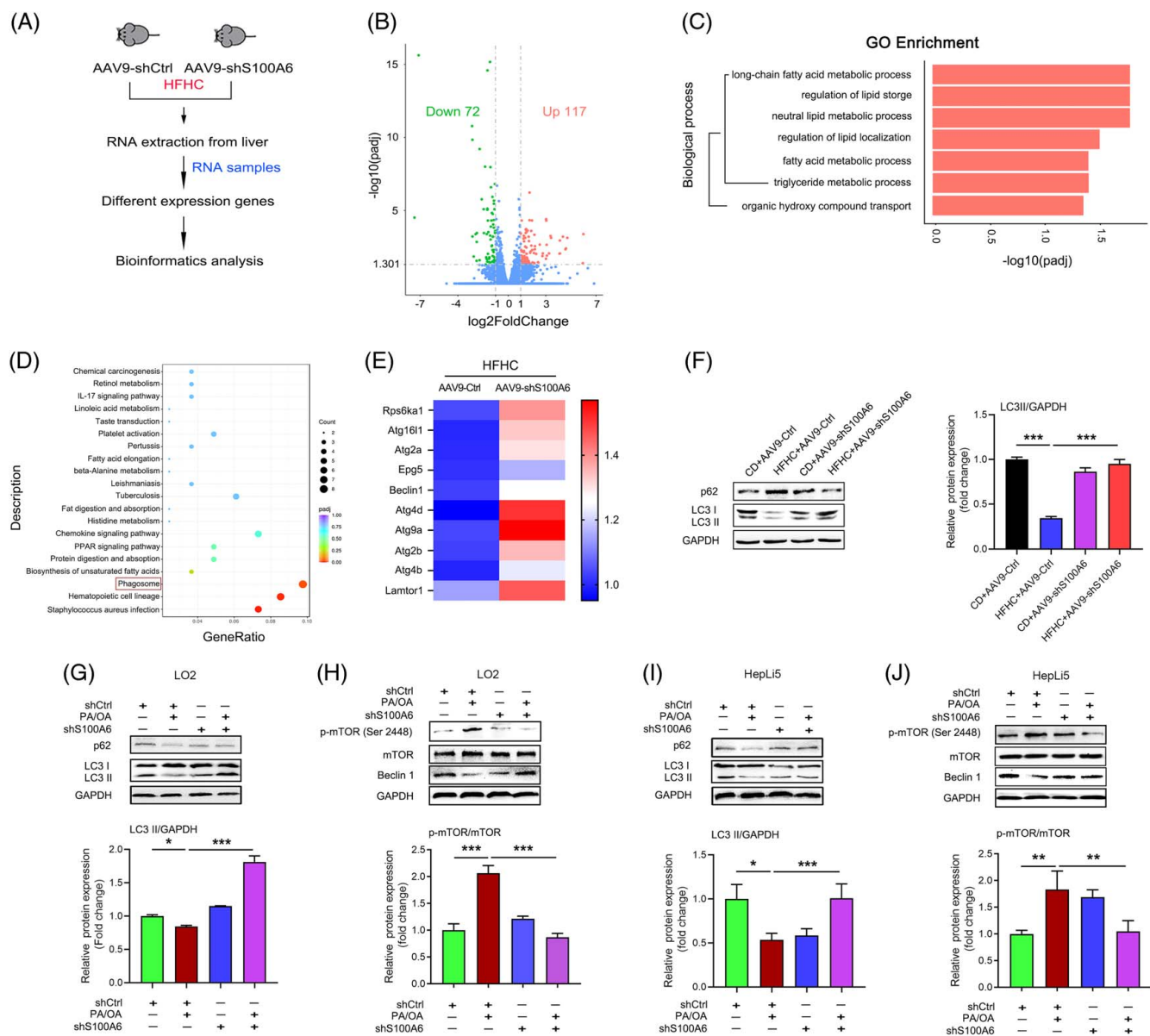
FIGURE 6 Hepatocyte S100A6 deficiency recovered autophagy after treatment with an HFHC diet or PA/OA. (A) Schematic of RNA-seq analysis samples. C57BL/6J mice were injected with AAV9-Ctrl or AAV9-shS100A6 adeno-associated virus for 1 week followed by HFHC treatment for 14 weeks.(B) Volcano plots indicating the differentially expressed genes (differentially expressed genes: red, upregulated genes; green, downregulated genes) in the AAV9-shS100A6 group relative to the AAV9-Ctrl group fed an HFHC for 14 weeks according to a differentially expressed gene assay. (C) The top 7 enriched biological processes contributing to S100A6 function were determined by GO analysis based on the differentially expressed genes from the differentially expressed gene assay. (D) Gene ratio enrichment of HFHC diet-induced AAV9-Ctrl or AAV9-shS100A6 mice. (E) Heatmaps of autophagy-related genes involved in HFHC-induced AAV9-Ctrl or AAV9-shS100A6 mice from RNA-Seq analysis. (F) Protein levels of LC3II and p62 in AAV9-Ctrl or AAV9-shS100A6 mice fed a CD or HFHC diet. (G) Protein levels of LC3II and p62 in S100A6 knockdown or control LO2 cells treated with PA/OA. (H) Protein levels of p-mTOR, mTOR, and Beclin1 in S100A6 knockdown or control LO2 cells treated with PA/OA. (I) Protein levels of LC3II and p62 in S100A6 knockdown or control HepLi5 cells treated with PA/OA. (J) Protein levels of p-mTOR, mTOR, and Beclin1 in S100A6 knockdown or control HepLi5 cells treated with PA/OA. Data are expressed as the mean $\pm$ SEM. *$p < 0.05$, **$p < 0.01$, ***$p < 0.001$. Abbreviations: CD, chow diet; GO, gene ontology, HFHC, high-fat high-cholesterol; OA, oleic acid; PA, palmitic acid.

Furthermore, we explored the autophagy flow in shS100A6 LO2 and HepLi5 cells, and found that CQ treatment had no effect on PA/OA-induced LC3II and p62 expression, suggesting that PA/OA stimulation blocked autophagy flow, which may result in the inhibition of LD uptake by autophagy (Figures S5H-S5M, http://links.lww. com/HC9/A453). Next, we found that LC3II accumulation under CQ treatment significantly increased after S100A6 knockdown. Surprisingly, the expression levels of LC3II in the shS100A6 cells treated with PA/OA and CQ were significantly higher than those in the control cells (Figure 7A and B). In addition, GFP-LC3 levels also
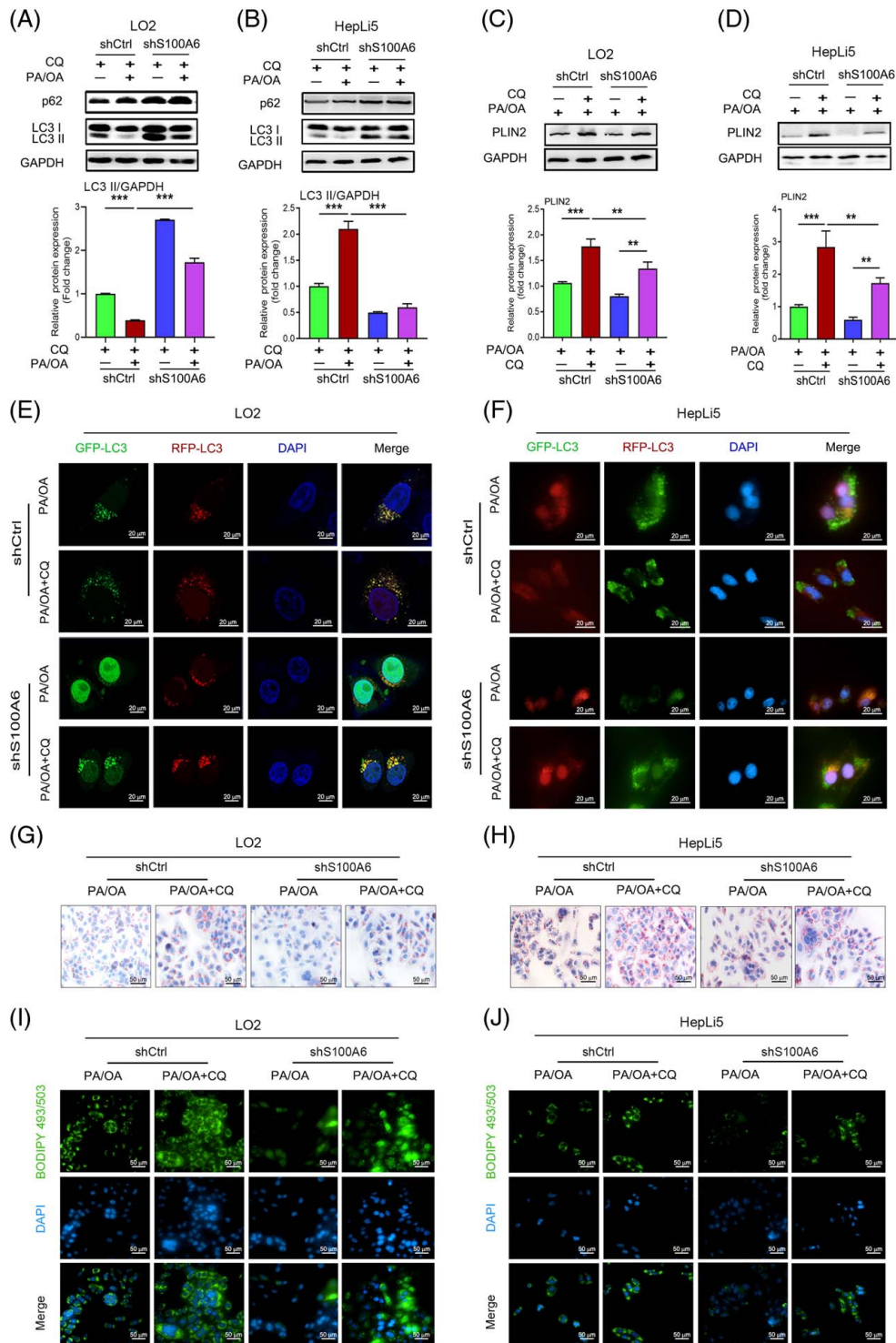
FIGURE 7 S100A6 knockdown promoted lipid metabolism by enhancing autophagic flow. Protein levels of LC3II and p62 in S100A6 knockdown or control LO2 cells (A) or HepLi5 cells (B) treated with CQ and/or PA/OA. Protein levels of PLIN2 in S100A6 knockdown or control LO2 cells (C) or HepLi5 cells (D) treated with CQ and/or PA/OA. Confocal images of S100A6 knockdown or control LO2 cells (E) and HepLi5 cells (F) transiently expressing mCherry-LC3 and GFP-LC3. Cells were treated with PA/OA and/or CQ. Representative Oil Red O staining images in LO2 cells (G) and HepLi5 cells (H). Representative BODIPY 493/503 images in LO2 cells (I) and HepLi5 cells (J). Data are expressed as the mean $\pm$ SEM. $^*p < 0.05$, $^{**}p < 0.01$, $^{***}p < 0.001$. Abbreviations: CQ, chloroquine; OA, oleic acid; PA, palmitic acid.

showed a higher autophagy flow in S100A6 cells treated with PA/OA, and the autophagy-related processes, such as the upregulation of mTOR phosphorylation during PA/ OA treatment, were significantly reversed after S100A6 knockdown (Figure 6H and J, Figures S5N and S5O, http://links.lww.com/HC9/A453, Figure 7E and F).
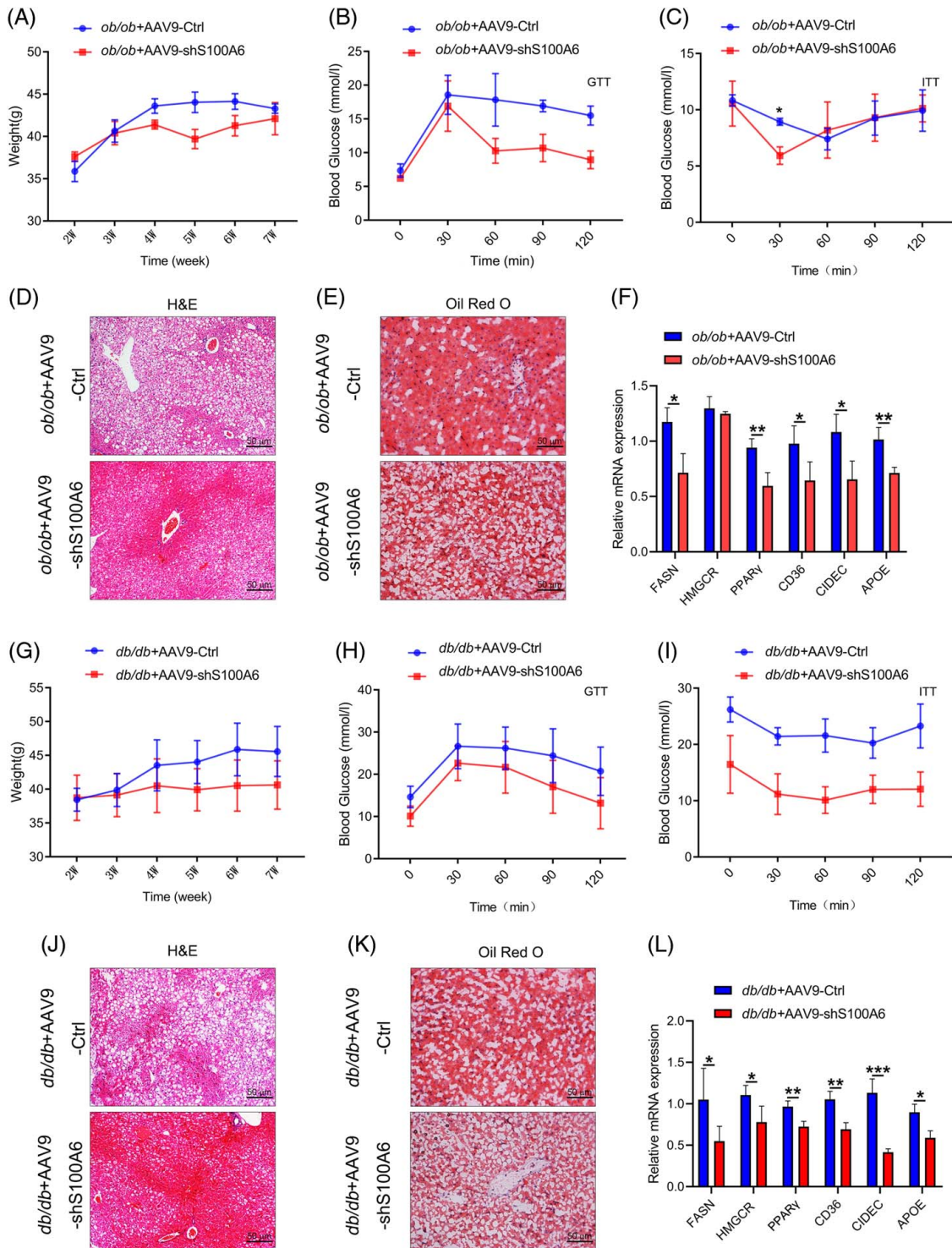
FIGURE 8 S100A6 knockdown attenuated hepatic steatosis and insulin resistance in *ob/ob* and *db/db* mice. (A) The body weights of *ob/ob* mice at 2, 3, 4, 5, 6, and 7 weeks after AAV9-Ctrl and AAV9-shS100A6 injection. GTTs (B) and ITTs (C) of *ob/ob* mice after AAV9-Ctrl and AAV9-shS100A6 injection. Representative images of H&E-stained (D) and Oil Red O-stained (E) liver sections from *ob/ob* mice injected with AAV9-Ctrl and AAV9-shS100A6. (F) The relative mRNA levels of lipid metabolic genes in *ob/ob* mice injected with AAV9-Ctrl and AAV9-shS100A6. (G) The body weight of *db/db* mice at 2, 3, 4, 5, 6, and 7 weeks after AAV9-Ctrl and AAV9-shS100A6 injection. GTTs (H) and ITTs (I) of *db/db* mice after AAV9-Ctrl and AAV9-shS100A6 injection. Representative images of H&E-stained (J) and Oil Red O-stained (K) liver sections from *db/db* mice injected with AAV9-Ctrl and AAV9-shS100A6. (L) The relative mRNA levels of lipid metabolic genes in *db/db* mice injected with AAV9-Ctrl and AAV9-shS100A6. Abbreviations: GTT, glucose tolerance tests; ITT, insulin tolerance tests.

Therefore, we decided to focus on whether S100A6 regulates lipid metabolism through autophagy. Significant LD accumulation was observed in PA/OA-treated cells under CQ treatment. In contrast, CQ reduced the accumulation of PA/OA-induced LDs in S100A6-knockdown cells (Figure 7G–J). Consistent with these findings, after CQ administration, the intracellular TG levels were significantly reduced in PA/OA-induced S100A6-knockdown cells (Figures S5P and S5Q, http://links.lww.com/HC9/A453). The level of PLIN2, a gene that mediates the degradation of LD through the autophagic pathway, was sharply decreased in PA/OA-induced S100A6-knockdown cells treated with CQ compared with that in control cells (Figure 7C, D). Overall, all these data suggest that S100A6 promotes lipid accumulation by activating the mTOR pathway and thereby regulating and suppressing the autophagy pathway.

Hepatocyte S100A6 deficiency ameliorated hepatic insulin resistance and steatosis in obese mice

To further determine whether our findings have potential translational importance, we performed 2 independent sets of experiments to evaluate S100A6 knockdown in the liver by means of tail vein injection of AAV9 expressing S100A6 shRNA, which can attenuate NAFLD in mice. First, 7-week-old *ob/ob* mice were subjected to tail vein injection of AAV9-Ctrl or AAV9-S100A6, followed by CD feeding for another 7 weeks. As shown in Figure S6A, http://links.lww.com/HC9/A453, the expression of S100A6 was significantly downregulated in the liver after AAV9-shS100A6 injection. S100A6 knockdown resulted in body weight reduction (Figure 8A). In addition, the i.p. glucose tolerance test and i.p. insulin tolerance test (Figure 8B and C) assays, and glycogen levels were markedly ameliorated in S100A6 knockdown mice (Figure S6B, http://links.lww.com/HC9/A453). Less lipid accumulation in the liver tissue of S100A6 knockdown mice was revealed by the H&E and Oil Red O staining results (Figure 8D and E), qPCR analysis results showed significant downregulation of lipid metabolism-related genes (Figure 8F).

Moreover, we tested the effects of S100A6 knockdown on the development of NAFLD in *db/db* mice. AAV9-S100A6 shRNA injection downregulated S100A6 expression in *db/db* mice (Figure S6C, http://links.lww.com/HC9/A453). Similar to these findings from the *ob/ob* mice, S100A6 knockdown ameliorated glucose tolerance, insulin tolerance, glycogen content, and downregulated lipid metabolism markers (Figure 8G–I and L) in the livers of the *db/db* mice. These data were supported by the H&E and Oil Red O staining results (Figure 8J and K). Taken together, these results indicate that hepatocyte S100A6 deficiency can reverse hepatic insulin resistance and steatosis in *ob/ob* mice.

DISCUSSION

In the current study, we identified a previously unknown role of S100A6 in liver steatosis, obesity-related insulin resistance, and inflammation at the clinical, cellular, and animal levels. First, the expression of S100A6 protein in the livers of patients with NAFLD and mice with liver steatosis was significantly increased. Second, S100A6 deficiency in hepatocytes largely protected against HFHC-induced fatty liver in mice. Third, the depletion of hepatic S100A6 attenuated hepatic steatosis in *ob/ob* and *db/db* mice. Furthermore, the underlying mechanisms demonstrated that S100A6 mediated hepatic steatosis by impairing lipophagy. This study demonstrates that the S100A6-lipophagy pathway may be a useful therapeutic target for the treatment of hepatic steatosis.

The incidence of NAFLD has been growing worldwide due to the prevalence of obesity and metabolic disorders. However, the pathogenesis of NAFLD is complex and multi-factorial, and the underlying molecular mechanisms remain largely unclear. In hepatocytes, cytoplasmic calcium is an important signal molecule that mediates physiological and pathological activities, including lipid metabolism and bile secretion.[25,26] Studies have shown that the imbalance of intracellular calcium homeostasis was the main cause of endoplasmic reticulum stress caused by liver lipid accumulation.[27–29] When the concentration of intracellular calcium ions increased in response to specific stimuli, S100 proteins bind to Ca^{2+}, and function as Ca^{2+} signal transducers to regulate many cellular functions.[30,31] In recent studies, the S100 proteins were identified as critical regulators of cellular events involved in multiple liver diseases, including NAFLD, NASH, fibrosis, and HCC.[32] S100A4 was reported to function in the regulation of HSC activation in liver fibrosis and HCC metastasis.[33–35] In addition, S100A8/A9 triggers distinct pathogenic processes in the liver tissue that together exacerbates steatosis-to-NASH progression, neutrophil recruitment, liver injury, and malignant progression of liver carcinogenesis.[36,37] S100A11 regulates lipid metabolism through AKT-mTOR/autophagy, liver fibrogenesis by targeting TGF-β signaling, and NASH-driven HCC development.[38–41] While an increasing number of studies have focused on the role of S100 proteins in regulating multiple critical signaling pathways, the potential role of S100A6 in the liver, especially in NAFLD, remains uncharacterized. This study revealed, for the first time, that S100A6 expression was significantly upregulated in multiple models of NAFLD, indicating the potential role of S100A6 in hepatic steatosis-related diseases In addition, using AAV9-mediated delivery of S100A6 deficiency into the livers of *ob/ob* and *db/db* mice, it was found that hepatic S100A6 deficiency markedly alleviated obesity-related hepatic steatosis, and insulin

resistance. Notably, the function of hepatic S100A6 was not only limited to the liver but also expanded to the other system, including serum glucose, insulin resistance, circulating lipid disorder, and obesity. These interesting results indicate another effect of hepatic modulation by S100A6. Thus, this study suggested that S100A6 may be a promising clinical therapeutic target for the prevention of hepatic metabolic disorders in the future.

Autophagy is a cellular self-digestion process in which a lysosomal-mediated pathway degrades intracellular organelles to maintain energy homeostasis.[42] Specially, the autophagy of hepatocyte LDs is an important way to maintain lipid homeostasis.[22,23] In NAFLD, disruptions in the components of the autophagic pathway could indeed promote hepatic lipid accumulation. A study from Yu Gao et al[12] showed that exercise directly increased lipophagy by activating the AMPK/ULK1 pathway, while dietary intervention decreased lipophagy through the Akt/mTOR/ULK1 pathway. mTOR is one of the most important signal molecules regulating autophagy, and our results supported this notion by demonstrating that S100A6 knockdown in hepatocytes obviously inhibited the mTOR signal pathway and promoted autophagy under PA/OA or HFHC administration. Interestingly, we found that lipid accumulation in normal hepatocytes may result in a clear barrier of LDs by autophagy, and we further confirmed that knockout of S100A6 itself could enhance autophagic flow by using CQ, and our RNA-Seq data analysis showed that the majority of genes involved in autophagic vesicles were upregulated in the HFHC+shS100A6 group compared to the HFHC+GFP group. These observations are consistent with previous studies demonstrating that the autophagic flux is impaired in the livers of NAFLD model mice.[10,43] S100A6 knockdown in hepatocytes could reverse the downregulation of LC3II expression and the defective autophagic flow induced by PA/OA treatment. In our studies, we further investigated whether S100A6 deficiency reduced the accumulation of PA/OA-induced LDs by increasing autophagy. Indeed, enhanced autophagic flux reduced the accumulation of PA/OA-induced LDs in S100A6 knockdown cells. PLIN2, the major perilipin on the surface of the LDs, can mediate the degradation of LD through the lipophagy.[44] In our study, the enhanced lipophagy in shS100A6 hepatocytes treated with PA/OA was also further confirmed by the LD marker PLIN2 level. Overall, these results suggested that S100A6 deficiency prevented HFHC-induced NAFLD by inducing lipophagy.

In summary, this study demonstrated the role of the S100A6-lipophagy axis in the regulation of lipid metabolism and the progression of NAFLD. Approaches that improve lipid metabolism by manipulating molecules, such as downregulating S100A6 expression, might be a promising strategy to rebalance lipid metabolism. Overall, targeting S100A6 is an attractive approach for the treatment of metabolic disorders and liver-related diseases such as liver steatosis and type 2 diabetes mellitus.

AUTHOR CONTRIBUTIONS
Qian Du and Tingting Zhu designed the experiments. Qian Du carried out most experiments and data analysis, Jiaxing An, Jingyu Xu, Rui Xie, Guorong Wen, Hai Jin, Jiaxing Zhu, Ting Zhang, Qi Liu, Shun Yao, and Xingyue Yang performed the experiments and analyzed the data; Qian Du and Tingting Zhu designed and drafted the manuscript; Biguang Tuo and Xiong Ma supervised this work.

CONFLICTS OF INTEREST
The authors have no conflicts to report.

DATA AVAILABILITY
Data that support the findings of this study are available from the corresponding author upon reasonable request.

ORCID
Qian Du https://orcid.org/0000–0001–7056–5208
Jingyu Xu https://orcid.org/0000–0002–0545–0444
Rui Xie https://orcid.org/0000–0003–3643–3388
Xiaoxu Yang https://orcid.org/0000–0002–6261–9867
Ting Zhang https://orcid.org/0000–0002–8270–708X
Qi Liu https://orcid.org/0000–0002–4876–2405

REFERENCES
1. Younossi Z, Anstee QM, Marietti M, Hardy T, Henry L, Eslam M, et al. Global burden of NAFLD and NASH: trends, predictions, risk factors and prevention. Nat Rev Gastroenterol Hepatol. 2018;15:11–20.
2. Byrne CD, Targher G. NAFLD: a multisystem disease. J Hepatol. 2015;62(1 Suppl):S47–64.
3. Liu Z, Zhang Y, Graham S, Wang X, Cai D, Huang M, et al. Causal relationships between NAFLD, T2D and obesity have implications for disease subphenotyping. Nat Rev Gastroenterol Hepatol. 2020;73:263–76.
4. Targher G, Corey KE, Byrne CD, Roden M. The complex link between NAFLD and type 2 diabetes mellitus - mechanisms and treatments. Nat Rev Gastroenterol Hepatol. 2021;18:599–612.
5. Jenkins CM, Mancuso DJ, Yan W, Sims HF, Gibson B, Gross RW. Identification, cloning, expression, and purification of three novel human calcium-independent phospholipase A2 family members possessing triacylglycerol lipase and acylglycerol transacylase activities. J Biol Chem. 2004;279:48968–75.
6. Villena JA, Roy S, Sarkadi-Nagy E, Kim KH, Sul HS. Desnutrin, an adipocyte gene encoding a novel patatin domain-containing protein, is induced by fasting and glucocorticoids: ectopic expression of desnutrin increases triglyceride hydrolysis. J Biol Chem. 2004;279:47066–75.
7. Zimmermann R, Strauss JG, Haemmerle G, Schoiswohl G, Birner-Gruenberger R, Riederer M, et al. Fat mobilization in adipose tissue is promoted by adipose triglyceride lipase. Science. 2004; 306:1383–6.

8. Onal G, Kutlu O, Gozuacik D, Dokmeci Emre S. Lipid droplets in health and disease. Lipids Health Dis. 2017;16:128.

9. Olzmann JA, Carvalho P. Dynamics and functions of lipid droplets. Nat Rev Mol Cell Biol. 2019;20:137–55.

10. González-Rodríguez Á, Mayoral R, Agra N, Valdecantos MP, Pardo V, Miquilena-Colina ME, et al. Impaired autophagic flux is associated with increased endoplasmic reticulum stress during the development of NAFLD. Cell Death Dis. 2014;5: e1179.

11. Zhang H, Lu J, Liu H, Guan L, Xu S, Wang Z, et al. Ajugol enhances TFEB-mediated lysosome biogenesis and lipophagy to alleviate non-alcoholic fatty liver disease. Pharmacol Res. 2021;174:105964.

12. Gao Y, Zhang W, Zeng LQ, Bai H, Li J, Zhou J, et al. Exercise and dietary intervention ameliorate high-fat diet-induced NAFLD and liver aging by inducing lipophagy. Redox Biol. 2020;36:101635.

13. Byrnes K, Blessinger S, Bailey NT, Scaife R, Liu G, Khambu B. Therapeutic regulation of autophagy in hepatic metabolism. Acta Pharm Sin B. 2022;12:33–49.

14. Li P, Lv X, Zhang Z, Xie S. S100A6/miR193a regulates the proliferation, invasion, migration and angiogenesis of lung cancer cells through the P53 acetylation. Am J Transl Res. 2019;11: 4634–49.

15. Song D, Xu B, Shi D, Li S, Cai Y. S100A6 promotes proliferation and migration of HepG2 cells via increased ubiquitin-dependent degradation of p53. Open Med (Wars). 2020;15:317–26.

16. Donato R, Sorci G, Giambanco I. S100A6 protein: functional roles. Cell Mol Life Sci. 2017;74:2749–60.

17. Wang XH, Du H, Li L, Shao DF, Zhong XY, Hu Y, et al. Increased expression of S100A6 promotes cell proliferation in gastric cancer cells. Oncol Lett. 2017;13:222–30.

18. Al-Ismaeel Q, Neal CP, Al-Mahmoodi H, Almutairi Z, Al-Shamarti I, Straatman K, et al. ZEB1 and IL-6/11-STAT3 signalling cooperate to define invasive potential of pancreatic cancer cells via differential regulation of the expression of S100 proteins. Br J Cancer. 2019;121:65–75.

19. Hu Y, Zeng N, Ge Y, Wang D, Qin X, Zhang W, et al. Identification of the Shared gene signatures and biological mechanism in Type 2 diabetes and pancreatic cancer. Front Endocrinol (Lausanne). 2022;13:847760.

20. Busch AK, Cordery D, Denyer GS, Biden TJ. Expression profiling of palmitate- and oleate-regulated genes provides novel insights into the effects of chronic lipid exposure on pancreatic beta-cell function. Diabetes. 2002;51:977–87.

21. Pan X, Li J, Du W, Yu X, Zhu C, Yu C, et al. Establishment and characterization of immortalized human hepatocyte cell line for applications in bioartificial livers. Biotechnol Lett. 2012;34:2183–90.

22. Filali-Mouncef Y, Hunter C, Roccio F, Zagkou S, Dupont N, Primard C, et al. The ménage à trois of autophagy, lipid droplets and liver disease. Autophagy. 2022;18:50–72.

23. Allaire M, Rautou PE, Codogno P, Lotersztajn S. Autophagy in liver diseases: Time for translation? J Hepatol. 2019;70:985–98.

24. Ueno T, Komatsu M. Autophagy in the liver: functions in health and disease. Nat Rev Gastroenterol Hepatol. 2017;14:170–84.

25. Maus M, Cuk M, Patel B, Lian J, Ouimet M, Kaufmann U, et al. Store-operated Ca(2+) entry controls induction of lipolysis and the transcriptional reprogramming to lipid metabolism. Cell Metab. 2017;25:698–712.

26. Ali ES, Petrovsky N. Calcium signaling as a therapeutic target for liver steatosis. Trends Endocrinol Metab. 2019;30:270–81.

27. Ali ES, Rychkov GY, Barritt GJ. Metabolic disorders and cancer: hepatocyte store-operated Ca(2+) channels in nonalcoholic fatty liver disease. Adv Exp Med Biol. 2017;993:595–621.

28. Zhang B, Li M, Zou Y, Guo H, Zhang B, Xia C, et al. NFκB/Orai1 Facilitates Endoplasmic Reticulum Stress by Oxidative Stress in the Pathogenesis of Non-alcoholic Fatty Liver Disease. Front Cell Dev Biol. 2019;7:202.

29. Ogino N, Miyagawa K, Kusanaga M, Hayashi T, Minami S, Oe S, et al. Involvement of sarco/endoplasmic reticulum calcium ATPase-mediated calcium flux in the protective effect of oleic acid against lipotoxicity in hepatocytes. Exp Cell Res. 2019;385:111651.

30. Chin D, Means AR. Calmodulin: a prototypical calcium sensor. Trends Cell Biol. 2000;10:322–8.

31. Donato R, R. Cannon B, Sorci G, Riuzzi F, Hsu K, J. Weber D, et al. Functions of S100 proteins. Curr Mol Med. 2013;13:24–57.

32. Delangre E, Oppliger E, Berkcan S, Gjorgjieva M, Correia de Sousa M, Foti M. S100 proteins in fatty liver disease and hepatocellular carcinoma. Int J Mol Sci. 2022;23:11030.

33. Chen L, Li J, Zhang J, Dai C, Liu X, Wang J, et al. S100A4 promotes liver fibrosis via activation of hepatic stellate cells. J Hepatol. 2015;62:156–64.

34. Sun H, Wang C, Hu B, Gao X, Zou T, Luo Q, et al. Exosomal S100A4 derived from highly metastatic hepatocellular carcinoma cells promotes metastasis by activating STAT3. Signal Transduct Target Therapy. 2021;6:187.

35. Rodrigues RM, He Y, Hwang S, Bertola A, Mackowiak B, Ahmed YA, et al. E-selectin-dependent inflammation and lipolysis in adipose tissue exacerbate steatosis-to-NASH progression via S100A8/9. Cell Mol Gastroenterol Hepatol. 2022;13:151–71.

36. Moles A, Murphy L, Wilson CL, Chakraborty JB, Fox C, Park EJ, et al. A TLR2/S100A9/CXCL-2 signaling network is necessary for neutrophil recruitment in acute and chronic liver injury in the mouse. J Hepatol. 2014;60:782–91.

37. Németh J, Stein I, Haag D, Riehl A, Longerich T, Horwitz E, et al. S100A8 and S100A9 are novel nuclear factor kappa B target genes during malignant progression of murine and human liver carcinogenesis. Hepatology. 2009;50:1251–62.

38. Teng F, Jiang J, Zhang J, Yuan Y, Li K, Zhou B, et al. The S100 calcium-binding protein A11 promotes hepatic steatosis through RAGE-mediated AKT-mTOR signaling. Metabolism. 2021;117:154725.

39. Zhang L, Zhang Z, Li C, Zhu T, Gao J, Zhou H, et al. S100A11 promotes liver steatosis via FOXO1-mediated autophagy and lipogenesis. Gut. 2021;11:697–724.

40. Zhu T, Zhang L, Li C, Tan X, Liu J, Li H, et al. The S100 calcium binding protein A11 promotes liver fibrogenesis by targeting TGF-β signaling. J Genet Genomics. 2022;49:338–49.

41. Sobolewski C, Abegg D, Berthou F, Dolicka D, Calo N, Sempoux C, et al. S100A11/ANXA2 belongs to a tumour suppressor/oncogene network deregulated early with steatosis and involved in inflammation and hepatocellular carcinoma development. Gut. 2020;69:1841–54.

42. Mizushima N, Komatsu M. Autophagy: renovation of cells and tissues. Cell. 2011;147:728–41.

43. Liu K, Qiu D, Liang X, Huang Y, Wang Y, Jia X, et al. Lipotoxicity-induced STING1 activation stimulates MTORC1 and restricts hepatic lipophagy. Autophagy. 2022;18:860–76.

44. Schulze RJ, Drižytė K, Casey CA, McNiven MA. Hepatic lipophagy: new insights into autophagic catabolism of lipid droplets in the liver. Hepatol Commun. 2017;1:359–69.